Application of boron oxide as a protective surface treatment to decrease the air reactivity of carbon anodes

LABORATOIRE LIS D'INGÉNIERIE DE SURFACE

Ramzi Ishak[1,2], Donald Picard[2], Gaétan Laroche[1], Donald P. Ziegler[3] and Houshang Alamdari[1,2]

[1]Cente *Department of Mining, Metallurgical and Materials Engineering, Laval University, Quebec City, QC G1V 0A6, Canada; (G.L.)*
[2]*NSERC/Alcoa Industrial Research Chair MACE3 and Aluminum Research Centre—REGAL, Laval University, Quebec City, QC G1V 0A6, Canada*
[3]*Alcoa Primary Metals, Alcoa Technical Center, 100 Technical Drive, Alcoa Center*

ABSTRACT
The oxidation of a carbon anode with air and CO_2 occurs during the electrolysis of alumina in Hall-Héroult cells, resulting in a significant overconsumption of carbon and dusting. Boron is well known to decrease the rate of this reaction for graphite. In this work, the application of boron oxide has been investigated to evaluate its inhibition effect on the air oxidation reaction, and to provide an effective protection for anodes. Different methods of impregnation coating have been explored. Impregnated anode samples were gasified under air at 525°C according to the standard measurement methods. X-ray tomography was used to obtain the microstructural information of the samples before and after air-burning tests. The impregnated samples showed a very low oxidation reaction rate and dust generation.

KEYWORDS
Anode air reactivity; boron oxide anode coating; anode impregnation coating; anode sample gasification; computed tomography (CT)

CITATION
Ishak, R., Picard, D., Laroche, G., Ziegler, D., & Alamdari, H. (2017). Application of boron oxide as a protective surface treatment to decrease the air reactivity of carbon anodes. Metals, 7(3), 79.

This is the author's version of the original manuscript. The final publication is available at MDPI Link Online via doi:10.3390/met7030079

1 INTRODUCTION

Carbon anodes are consumed in the conventional process of aluminum production using Hall-Héroult cells in which the overall reaction may be written as Equation (1) [1]. One of the main factors causing excess anode consumption is oxidation of the anode surface exposed to air during electrolysis. The temperature of the anode exposed to air is between 400 and 600°C [2]. In this range, the oxygen in the air can react with the carbon anode, according to Equations (2) and (3). Both reactions are undesirable since the carbon anode is consumed without producing metal.

$$2Al_2O_3(diss) + 3C(s) \rightarrow 4Al(m) + 3CO_2(g), \Delta G^o = -339\ kJ\ (at\ 977°C) \quad (1)$$

$$C(solid, anode) + O_2(g) \rightarrow CO_2(g), \Delta G^o = -395\ kJ\ (at\ 500°C) \quad (2)$$

$$C(solid, anode) \rightarrow \frac{1}{2}O_2(g) + CO(g), \Delta G^o = -185\ kJ\ (at\ 500°C) \quad (3)$$

Air reactivity is one of the most important, variable characteristics of carbon anodes, and together with CO_2 reactivity counts as the highest contribution to carbon overconsumption. The anode is composed of calcined petroleum coke, recycled anodes (butts), and coal tar pitch. The effects of raw materials, process parameters, and the physical characteristics of the baked anode on its resistance against air reactivity have been widely discussed in the literature [3–8]. There is consensus that the burning rate of the binder matrix (pitch + fine) is higher than that of the large coke grains [8,9]. This may result in early removal of the binder matrix and detachment of the unburned coke grains from the anode surface, contributing in part to the dusting phenomenon [10–12]. Any protection strategy should therefore focus on providing an impermeable physical barrier on the anode external surface or decreasing the intrinsic reaction rate of carbon, especially that of the binder matrix.

Several attempts have been made to provide a physical barrier on the anode. As an example, the Commonwealth Scientific and Industrial Research Organisation (CSIRO) claimed to provide a cost-effective coating on anodes, which maintains its integrity throughout the life of the anode [13]. The coating seems to be an alumina-based material, which is sprayed on baked anodes. Although this announcement was made several years ago, the authors are not aware of any further development or industrial deployment of this coating. In the same context, covering the anode by alumina powder is practiced in almost all smelting plants. In addition, some plants practice a simple way to cover anodes by spreading liquid bath (cryolite) on a fresh anode just after it is changed. The liquid bath solidifies immediately on the cold anode surface providing a coating, which seems to decrease its air-burning rate. Both the alumina powder and solidified bath are porous media and cannot protect the anode efficiently. However, they may reduce the air-burning rate by generating an oxygen diffusion barrier around the anode and protect it to some extent.

Another strategy to protect carbon is to decrease its intrinsic reactivity. The oxidation inhibition is achieved by doping carbon with phosphorus and boron [14,15]. However, phosphorus is prohibited in the electrolysis bath due to its negative effect on the current efficiency, thus leaving only boron doping as a suitable strategy. Basically, three mechanisms are proposed to explain the effect of boron on the carbon oxidation reaction:

(a) Inhibition of the reaction by re-distribution of electron densities on graphite, hence reducing its intrinsic reactivity [16–19].

(b) Effect of boron on enhancing the graphitization process [17,19–21].

(c) Formation of the boron oxide film and blockage of active sites [16,22,23].

The two first mechanism (a and b) could not contribute to anode protection. The main reasons are:

(1) In most experimental works conducted on composite materials reinforced by carbon fiber, the boron addition level is too high (from 1000 ppm up to several at. %) [24]. This high level of boron addition is not allowed in the anode, keeping in mind that all boron will most likely reduce in the bath and enter the aluminum.

(2) The change in electron density is basically due to the fact that boron is substituted in the graphite structure. Since the anode baking temperature is much lower than the graphitization temperature, no significant graphitization occurs during baking. Thus, the boron effect on carbon graphitization is not conceivable.

(3) In boron-doped graphite, boron is always added in the form of elemental boron under inert atmosphere prior to graphitization. Considering the cost of elemental boron, such a high level of addition is justified only for very high-value products, which is not the case for carbon anodes.

The formation of the boron oxide film and its effect on active site blockage is, however, worth investigation.

Boron oxide is soluble in water, thus making it possible to be coated by impregnation via an aqueous solution. In this context, Moltech published four patents [25–28] about the impregnation coating of boron oxide to protect the anode. In these patents, the addition of other functional compounds into the impregnation solution was also claimed. The experiments conducted by Moltech in the laboratory seem to confirm the beneficial effect of this impregnation. Such a beneficial effect has also been confirmed by our own experiments, as well as by other authors [29]. However, the reasons why this technique has not been deployed in smelters, despite the good laboratory results, are unknown to the authors of this paper.

Alcan has also published a patent on the protection of anodes and cathodes by boron-containing compounds with different additives such as AlF_3 and refractory compounds [30]. The coating comprises "preparing a liquid suspension of a boron compound, aluminum fluoride and a lignosulfonate binder and applying the liquid suspension as a protective coating at least to the portion of the anode which is exposed to the atmosphere during cell operation, followed by drying the coating" [31]. They applied a thick coating layer using a spray gun followed by drying. They claimed a good protection of anodes and cathodes at the laboratory scale.

The laboratory tests are usually performed on small samples, referring to the standard test of R & D Carbon, typically 50 mm in diameter and 100 mm in length. The mass before and after the reaction is measured and the mass loss is reported as the indication of reactivity. Therefore, no information is obtained regarding the reaction kinetics or the evolution of the reaction over time. In addition, if the impregnation efficiency depends on the sample size, its protection capability will be overestimated for the small samples. It is thus important to understand the protection mechanism in order to adjust the process parameters for optimum performance.

This work aims at developing a protective coating to decrease the air reactivity of anodes. The focus is on determining the impregnation parameters that affect the efficiency of the process. During the reactivity tests, the mass loss is recorded continuously in order to follow the reaction rate at any time. The samples were also characterized using X-ray tomography in order to obtain the microstructural information before and after the air-burning tests. This information helped to understand the carbon gasification process inside the anode samples.

2 MATERIALS AND METHODS

2.1 Materials

In this study, all samples were taken from an industrial baked anode. The anode consisted of 65% calcined petroleum coke, 22% recycled anode and 13% pitch, and baked at 1200°C. The samples were cored from different parts of the anode. Most of the samples were taken from the positions that are normally exposed to air attack in an industrial electrolysis cell.

2.2 Air Reactivity Test

The air reactivity measurements were conducted using a muffle furnace. In the first series of experiments, a small sample of approximately 6–7 g was tested, while in the second and third series a larger sample size (60–100 g) was used. The samples were impregnated with boron solution under different conditions. The reactivity experiments were performed under isothermal conditions in flowing air of 4–5 L/min. The samples were protected from oxidation during the heating period by high purity nitrogen. When the target temperature was reached, the sample was held at this temperature for 10 min. Then, air was introduced into the reaction chamber. The sample was maintained at the target temperature before being cooled. During the cooling period, the sample was also protected from oxidation using a nitrogen flow. The anode-air reaction was measured over a range of temperatures from 400 to 600°C. This temperature range corresponds to the conditions in which the anode reacts with the air atmosphere during the aluminum smelting process.

2.3 X-ray Computed Tomography

X-ray computed tomography has been used for decades in science to reveal the internal structures of objects, from living beings to engineering materials (e.g., [31–34]) including the carbon materials used in the aluminum production industry [35–39]. Its main advantage is that it is a non-destructive technique. Thus, it can preserve object integrity such as porosity distribution. Hence, carbon anode images have been obtained by scanning anode cores before and after air reactivity tests using computed tomography (Siemens Somatom Sensation 64, Figure 1). This method is also capable of revealing the spatial density distribution in the sample. Considering the anode core dimension (50 mm in diameter), the voxel resolution obtained is 0.1x 0.1 x 0.6 mm^3 which is very close to the maximum resolution of the X-ray tomography used in this study (0.09 x 0.09 x 0.4 mm^3).

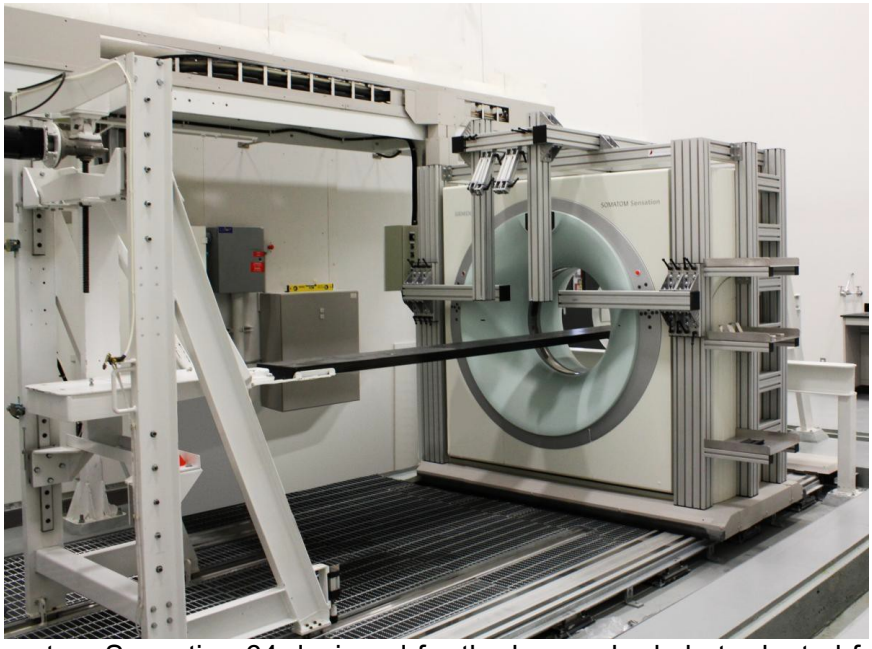

Figure 1. Siemens Somatom Sensation 64 designed for the human body but adapted for material research. Courtesy of INRS-ETE, Quebec, QC, Canada.

3 RESULTS AND DISCUSSION

3.1 Anode Impregnation

A series of small samples (6–7 g) were cut from an industrial anode core and impregnated under different conditions. The cored samples had a diameter of 19 mm and a length of 14 mm. The solution concentration and impregnation temperature were varied. The samples were dipped in the solution for 30 min, and then dried in air at 100°C overnight. Samples 1, 2, 3, 4 and 6 were impregnated for a second time under the same condition. Tables 1 and 2 summarize the treatment conditions of the 13 samples, including the references (untreated).

Table 1. Impregnation conditions of the samples.

Sample	Solute Mass (g)	Solvent	Solvent Volume (mL)	Concentration (g/mL)	Solution Temperature
A	Untreated	-	-	-	-
B	Untreated	-	-	-	-
C	Untreated	-	-	-	-
1	9	Water	50	0.180	Boiling
2	1	Water	50	0.020	R. temp
3	9.08	Water	50	0.182	Boiling
4	1	Water	50	0.020	R. temp
5	1	Water	50	0.020	R. temp
6	8.98	Water	50	0.180	Boiling
7	9.03	Water	50	0.181	Boiling
8	9.08	Water	50	0.182	Boiling
9	9.03	Water	50	0.181	Boiling
10	1.05	Water	50	0.021	R. temp

Table 2. Impregnation (2) conditions of the samples.

Sample	Solute Mass (g)	Solvent	Solvent Volume (mL)	Concentration (g/mL)	Solution Temperature
1	9.06	Water	50	0.181	Boiling
2	1.02	Water	50	0.020	R. temp
3	9.06	Water	50	0.181	Boiling
4	1.03	Water	50	0.020	R. temp
6	8.94	Water	50	0.179	Boiling

The air reactivity tests were performed in a muffle furnace with an airflow of about 5 L/min. The samples were put in the furnace, heated to 525°C and maintained at this temperature for 2 h. The temperature was then decreased to 500°C over 1 h and maintained at this temperature for 2 h. The temperature was then decreased to 450°C and maintained until the end of the test. Samples were then withdrawn from the furnace and weighed. The residue was calculated according to the following equation:

$$Air\ reactivity\ residue = \frac{M_f}{M_i} \times 100 \quad (4)$$

where M_f and M_i are the final and initial mass of the sample, respectively.

Figure 2 shows the air reactivity residue of the treated (1–10) and the untreated samples (A, B and C). The results confirmed that the boron treatment has a significant effect on the air reactivity of the anode samples. The untreated samples showed a high reactivity with a mass loss ranging between 52% and 75%. The impregnated samples showed much smaller mass loss between 4.5% and 11%. The best results were in general obtained for the samples impregnated in hot solution (7 and 9), although all of the treated samples seemed to be efficiently protected. Sample 1, 2, 3, 4 and

6 did not show any difference compared to the others, even with the double impregnation. Therefore, it seems that the anode surface was saturated with boron oxide during the first impregnation.

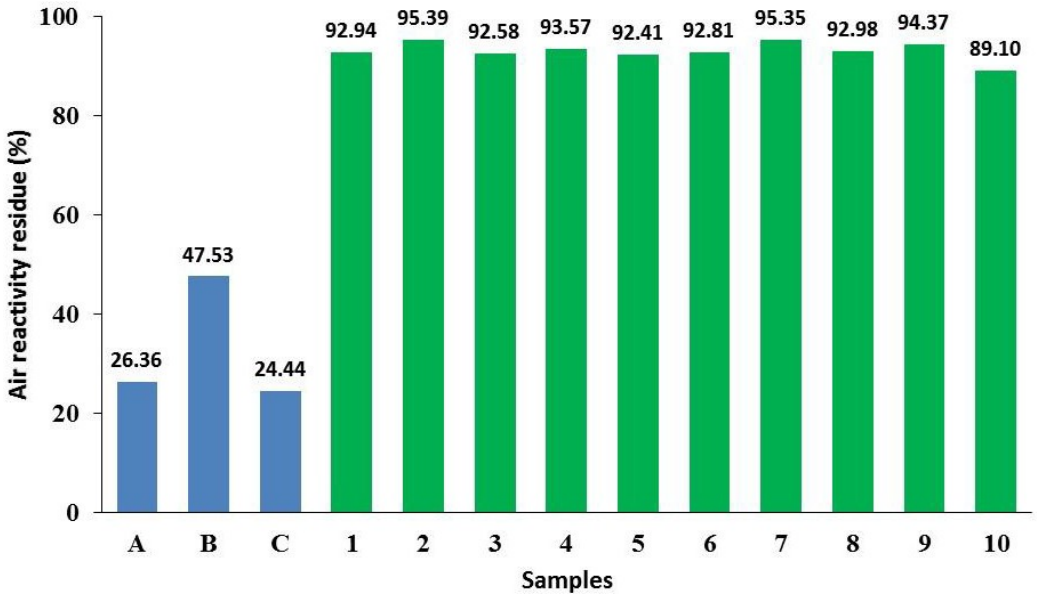

Figure 2. Air reactivity of the samples coated by impregnation.

3.2 Effect of impregnation time

In the second series of experiments, the effect of impregnation time was evaluated. Eight samples were cored from the same anode having a diameter of 50 mm and a length of 30 mm. The average mass of the samples was around 100 g. Samples were soaked in a boiling solution with a concentration of 0.17 g/mL using impregnation times varying between 1 and 20 min. The coating conditions of the samples are summarized in Table 3.

Table 3. Impregnation conditions of the samples.

Sample	Solute Mass (g)	Solvent	Solvent Volume (mL)	Concentration (g/mL)	Solution Temperature	Dipping Time (min)
1	Untreated	-	-	-	-	-
2	Untreated	-	-	-	-	-
3	53.49	Water	300	0.178	Boiling	1
4	53.49	Water	300	0.178	R. temp	10
5	48.08	Water	265	0.181	Boiling	1
6	48.08	Water	265	0.181	R. temp	10
7	35.87	Water	200	0.179	R. temp	20
8	36.19	Water	200	0.181	Boiling	20

The air reactivity tests were performed in a muffle furnace with an airflow rate of 4 L/min. The samples were put on an alumina wool, placed on a stainless-steel plate, and introduced in the furnace at 500°C. The temperature of the furnace was maintained at 500°C during the entire air reactivity test. In order to follow the reaction rate over time, the samples were removed from the furnace, cooled down to room temperature, weighed, and put back into the furnace. This operation was repeated every 2 h for the first 24 h and every 12 h for the remaining time. The gasification was calculated according to the following equation:

$$Gasification = \frac{M_0 - M_t}{M_o} \times 100 \quad (5)$$

where M_0 represents the initial weight of the sample and Mt is the instantaneous weight of the sample at time t.

The gasification percentage as a function of reaction time is shown in Figure 3. The results revealed a remarkable effect of the impregnation time on the air reactivity of the anode. The untreated anode shows high reactivity with a burning rate of about 4%/h. The anode was totally consumed after 40 h of reaction. The curves show that the reaction rate decreases by increasing the impregnation time. The resistance of the 1 min impregnated sample was almost doubled compared to that of the uncoated samples. The samples impregnated for 10 and 20 min showed lower reactivity with the same reaction rate (about 0.2%/h) and after 160 h they were consumed only by 70% and 60%, respectively. The reaction slightly accelerated for these samples after 20% gasification. As can be seen, the sample impregnated for 20 min exhibited a remarkable resistance to burning with only 30% mass loss after 100 h of reaction. Its reaction rate was 20 times lower than that of the untreated sample. The large standard deviation observed in this experiment could be attributed to the inhomogeneity of the anode and the small size of the samples.

Figure 4 shows a SEM (Scanning Electron Microscopy, JSM-840A, JEOL USA, Inc., Peabody, MA, USA) image of the cross section of an impregnated sample. One can observe lamellar boron oxide crystallized inside the pores. The protection effect can be explained by this observation, since boron blocks the pore surface and limits the access of oxygen. However, the relatively small areas covered by boron oxide cannot explain the significant decrease of the reaction rate. Boron oxide is likely also present on the other areas but, due to the limited resolution of SEM, it is not observed.

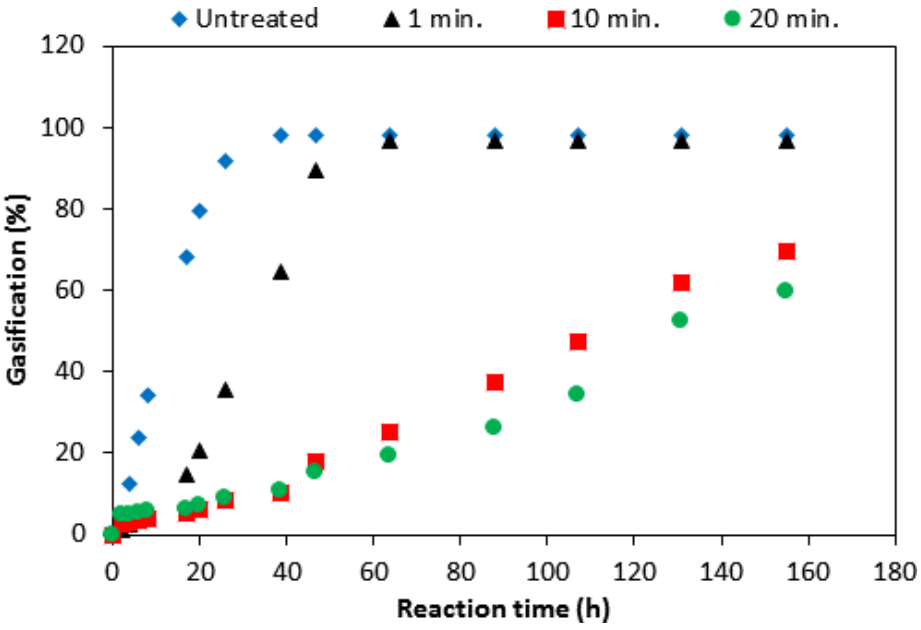

Figure 3. Gasification vs. reaction time during gasification for a series of samples with different impregnation times.

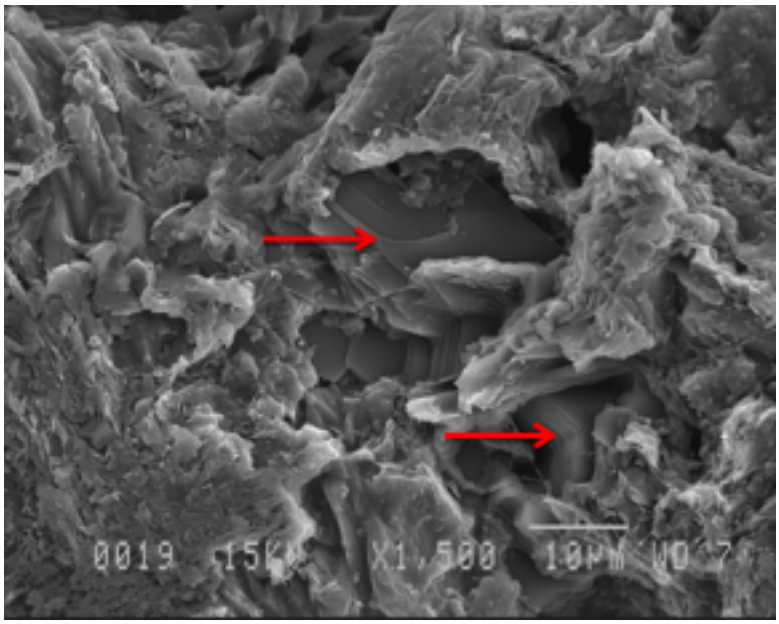

Figure 4. SEM micrograph of a sample cross-section showing the crystallization of boron oxide inside the pores (indicated by arrows).

Figure 5 shows visual aspects of the samples at different reaction times. Figure 5a–c shows the fresh samples, after 24 h and after 6 days of reaction, respectively. It can be clearly seen that the two reference samples (untreated) are severely reacted after 24 h of exposure, exhibiting a mass loss of more than 86%. The entire samples are disintegrated in powder form, which would be considered as dust in a real smelting pot. The mass loss measurements were stopped when the samples disintegrated. For this reason, the gasification never reached 100% (Figure 2).

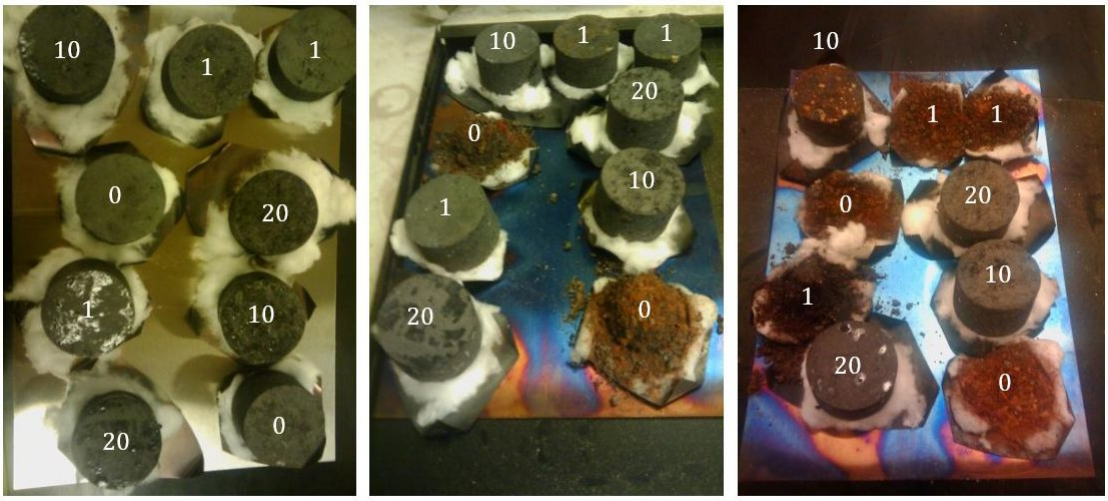

(a) (b) (c)

Figure 5. Visual observation of the samples; (a) before air reactivity test; (b) after 24 h of exposure; (c) after 6 days of exposure. The numbers on the samples indicate the impregnation time.

The visual inspection of the samples indicates that after only 24 h of exposure, the untreated samples are disintegrated while the sample impregnated for one minute still seems to be intact, although it exhibited 20% mass loss. This sample disintegrated after 40 h of exposure, generating a

large quantity of dust. After 6 days of exposure, however, the samples impregnated for 10 and 20 min kept their initial shape without any apparent dusting, in spite of more than 50% mass loss. This observation suggests that these samples essentially react from the inside while the outer surface is still resisting. This could mean that longer impregnation times not only decrease the overall reaction rate, but also decrease dust emission.

3.3 Boron loading during impregnation

Another series of large-size samples (50 mm in diameter) was prepared in order to obtain additional information about boron loading and its effect on air reactivity of the anode. The standard core samples of 50 mm diameter were cut into pieces of about 30 mm height. The same protocol of impregnation, as described previously, was used to impregnate the samples with two different impregnation times of 1 and 15 min. A boron solution at 2% and a temperature of 50°C was used for impregnation.

During the drying step of the impregnated sample, boron oxide is precipitated in the form of boron hydroxide. Depending on the drying temperature, boron hydroxide could be partially dehydrated to boron oxide. Thus, the evaluation of the exact boron quantity loaded on the sample becomes difficult. In order to overcome this difficulty, boron loading was calculated based on the weight of the impregnated solution. Knowing the concentration of the solution, it was possible to evaluate the exact boron quantity loaded on the sample during impregnation. To do so, the samples were first dried in an oven at 140°C for 4 h in order to record their initial dry weight. Then, a solution of a known boron concentration was prepared for impregnation. A sample was dipped into the solution and the difference between the weight of the solution before and after dipping was recorded. Table 4 summarizes the experimental conditions of the impregnation process as well as the quantity of boron oxide loaded onto each sample.

Two important observations were made at this step.

(1) The boron loading for a given impregnation time is different from one sample to another, ranging from 0.072 to 0.144 g for 10-min of impregnation and 0.074–0.157 g for 15 min of impregnation. The variation could be attributed to the different levels of porosity in the samples. This observation may explain the large variation in the reactivity of the samples, as observed for samples 10 and 20 in Figure 5, exhibiting different reactivity, in spite of the same impregnation time. Strictly speaking, this observation confirms that the boron loading could be different even if the impregnation conditions are the same.

(2) The average value of boron loading on two sets of samples (9–16 and 17–27) increased from 0.09 g to 0.13 g, respectively. This suggests that the average boron loading increases significantly by increasing the impregnation time.

Figure 6 shows the mass loss of the samples as a function of reaction time. The air reactivity tests were conducted in a muffle furnace with an airflow of 3 L/min at a constant temperature of 500 °C. To generate each point presented in this figure, several samples were placed in the furnace and, at each target exposure time, one sample was withdrawn from the furnace. Boron loading is indicated for each data point on the graph. The untreated samples showed the same reaction rate as observed previously in Figure 2. Once again, this series of experiments confirmed the positive effect of the long impregnation time on the air reactivity of anode samples.

Table 4. Boron loading on impregnated samples.

Sample	Dry Sample (g)	Beaker + Solution (g)	Solution in Sample (g)	B_2O_3 Loading (g)	Dipping Time (min)
-	-	701.0	-	-	-
9	74.2537	693.8	7.2	0.144	1
10	79.8949	689.4	4.4	0.088	1
11	76.9634	685.0	4.4	0.088	1
12	75.5964	679.9	5.1	0.102	1
13	75.3947	675.6	4.3	0.086	1
14	71.5214	671.2	4.4	0.088	1
15	74.0581	666.6	4.6	0.092	1
16	78.2129	663.0	3.6	0.072	1
-	-	682.0	-	-	-
17	78.3638	678.3	3.7	0.074	15
18	79.0604	670.5	7.8	0.156	15
19	62.7609	664.0	6.5	0.130	15
20	64.5848	657.4	6.6	0.132	15
21	59.4021	651.4	6	0.120	15
22	61.6083	643.8	7.6	0.152	15
23	61.8290	637.8	6.0	0.120	15
24	61.5569	630.3	7.5	0.150	15
25	68.1607	623.3	7	0.140	15
26	75.3353	615.4	7.9	0.158	15
27	74.0279	609.0	6.4	0.128	15

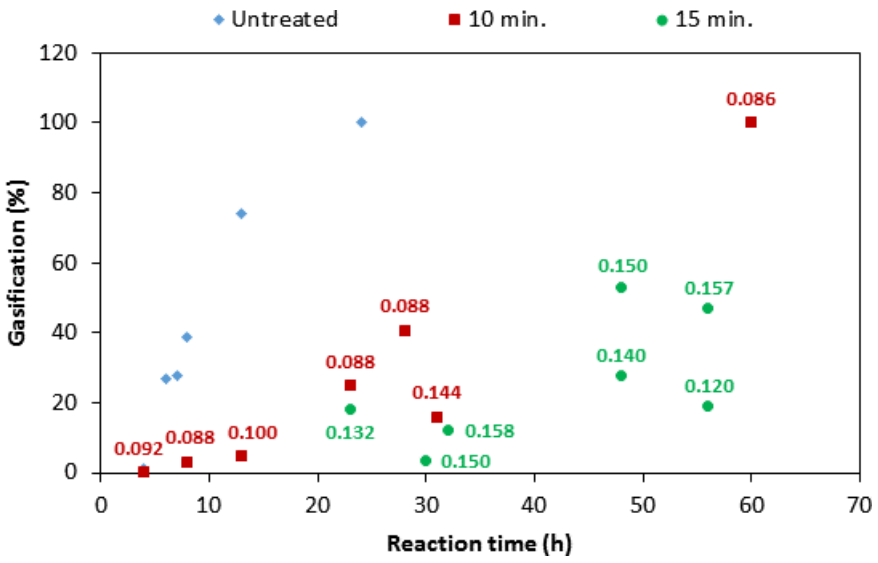

Figure 6. Gasification vs. reaction time during gasification for a series of samples with different boron loading.

3.4 Effect of boron-coating on the anode reaction mode

X-ray tomography was used in this study to obtain microstructural information of the samples before and after air reactivity tests. Two samples, impregnated and un-impregnated, were selected from those of the previous section (50 mm in diameter and a length of 30 mm) and were scanned before and after the air burning tests. This technique could show the evolution of the density by referring to the initial shape of the sample before and after air burning.

Figure 7a shows 16 images representing 16 equidistant scanned slices of an un-impregnated sample before the air reaction test, where the dark areas represent the pores. Scanning starts from the top of the sample (first image in the upper-left corner), and the bottom-right slice represents the bottom of the sample. Figure 7b shows the same sample after 6h of exposure, representing 27% mass loss. The top of the sample burns faster than the middle because the fresh air was injected from the top of the furnace. The bottom of the sample did not react at the same rate as the top because the sample was placed on alumina wool in which the air was not freely circulated.

Comparing the images before and after the air-burning test, it can be seen that the top surface of the sample (Figure 7b) was heavily attacked. Furthermore, the sample shrunk, indicating that it was basically attacked from its external surface. In order to better visualize the surface attack of the sample, the patterns of the burnt slices are superimposed on that of the fresh sample in Figure 8, where the shrinkage of the sample is clearly revealed. The level of porosity inside the sample remained roughly the same, which could reveal important information regarding the gas concentration through the pores. These results suggest that oxygen reacts quickly with carbon and that the CO_2/CO ratio falls rapidly inside the pores, preventing further reaction of the sample core. Such data indicate the importance of diffusion inside the pores in the anode reaction.

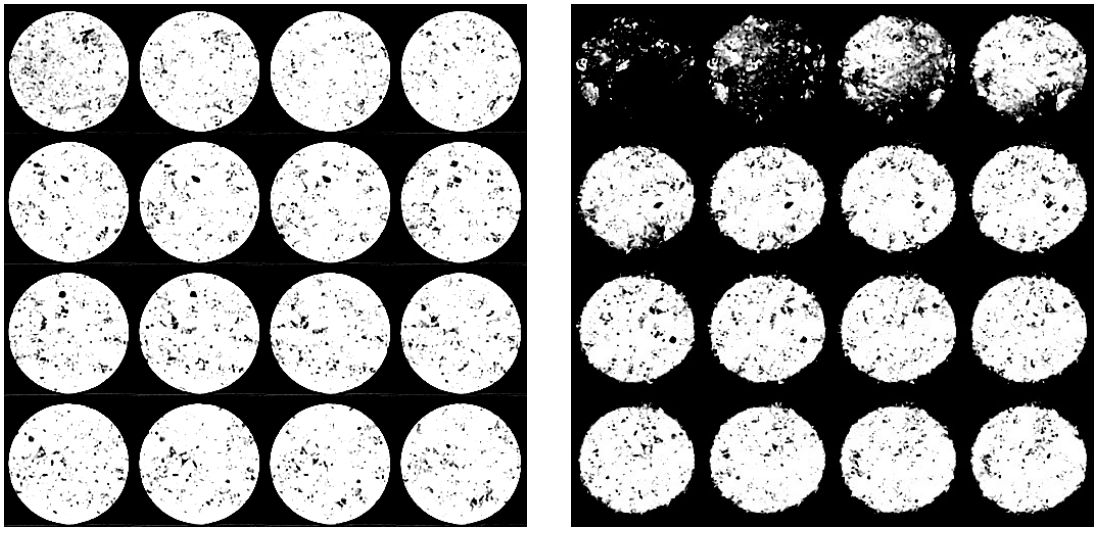

(a) (**b**)

Figure 7. X-ray tomography images of uncoated samples; (a) before air burning; (b) after 6 h of exposure at 500°C.

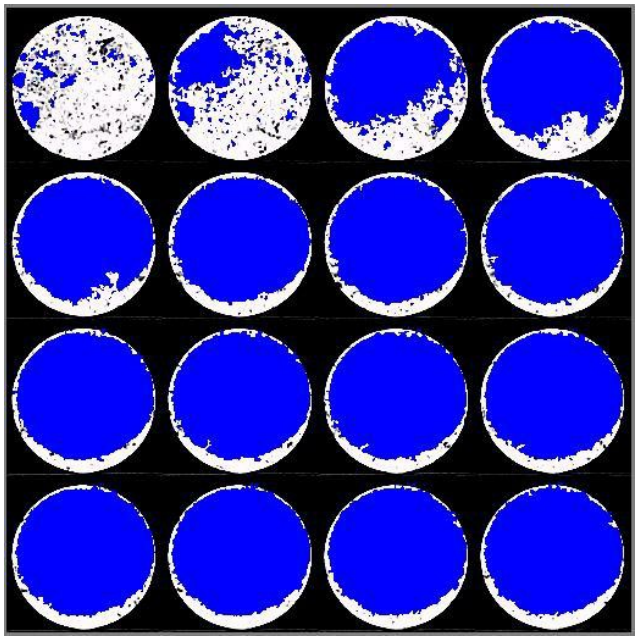

Figure 8. Superimposed patterns of the fresh (white) and burnt (blue) sample reveal the shrinkage of the sample after 6 h of exposure.

The impregnated sample was also scanned using X-ray tomography with the same parameters. Figure 9a shows the CT images taken from the sample before the air reactivity test. This sample was later impregnated for 15 min and exposed to air for 56 h in the furnace at 500°C. A mass loss of 19.3% was recorded after 56 h of exposure. The sample was again CT-scanned after air-burning test and the images are shown in Figure 9b. Compared with the uncoated sample, the impregnated sample did not shrink during the burning test and its diameter after burning remained the same as the fresh sample. Another interesting observation in Figure 9 is that the reaction took place inside the sample and only the porosity increased during the air-burning test.

It can be concluded from the reactivity tests and the CT scan results that the general oxidation resistance of an anode increases by boron impregnation and its surface is well protected. Localization of the air reaction to the inside of the impregnated sample core can be explained by the fact that oxygen diffuses through the pores, providing the reactant for oxidation. This means that the reaction will not become diffusion limited. In other words, due to the low intrinsic reactivity of the treated carbon, the CO_2/CO ratio does not decrease rapidly inside the sample and CO_2 (or oxygen) can reach the core of the sample. The low reaction rate of an impregnated sample could therefore be attributed to two facts:

(1) The impregnation solution reaches the entire pore network and provides a good protection even inside the sample.

(2) For the impregnated samples the reaction rate is very slow, so that the reaction will not be limited by diffusion. For the un-impregnated sample, however, diffusion limitation leads to consumption of only the outer surface.

In addition, the fact that the reacted samples preserve their integrity suggests that an impregnated anode will generate far less dust during the oxidation reaction.

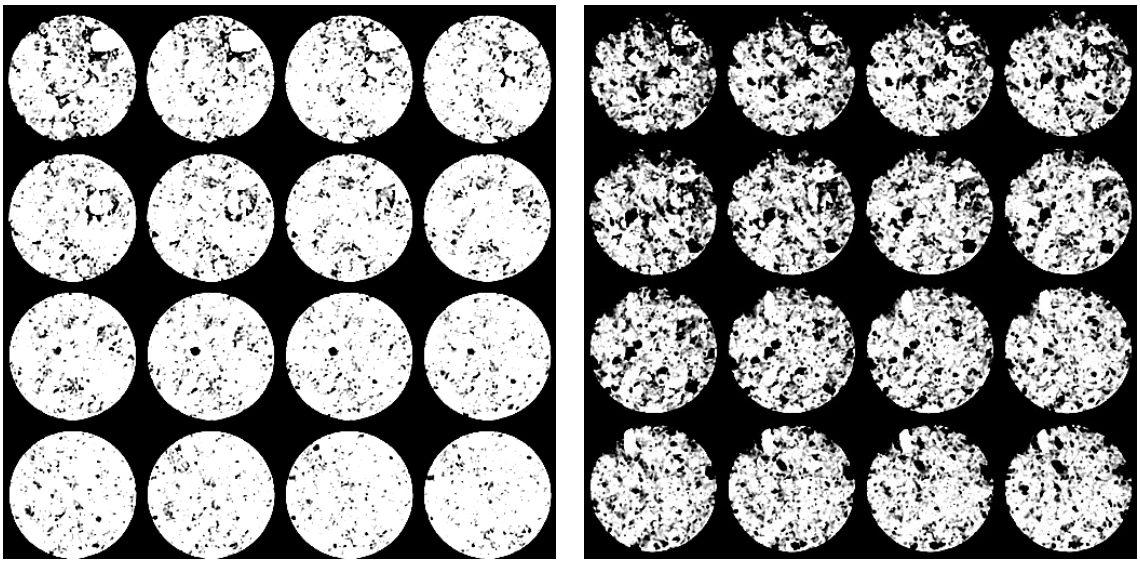

(a) (**b**)

Figure 9. Computed tomography (CT) scan images of a sample, (a) fresh; and (b) after impregnation for 15 min and exposure for 56 h at 500°C.

4 CONCLUSIONS

In the present study, it was shown that a number of parameters affect the efficiency of the anode protection by boron impregnation. For instance, the level of the protection depends on the impregnation duration. Fifteen minutes of impregnation in warm solution (2 wt % concentration) provides a significant protection level in small samples. Air reactivity results confirm that the protection of the anode surface using the impregnation method can decrease the oxidation reaction rate from 4%/h to 0.2%/h. CT-Scan results revealed that the inside of the impregnated samples seems to react with air, with a much slower rate, and that the surface preserves its initial shape. The protected samples generate much less dust as compared to the unprotected samples.

Although this technique allows us to obtain a very good anode protection and dust reduction, its implementation at the industrial scale may be challenging. Indeed, a full impregnation can be obtained within a reasonable time for small samples. In an industrial context, a full impregnation of an anode with a very large size would be practically impossible within a reasonable time. Accordingly, researchers and engineers will have to continue working on this avenue in order to find a practical method for in-depth impregnation of the large anode blocks.

ACKNOWLEDGEMENTS

The authors would like to acknowledge the financial support of the Natural Sciences and Engineering Research Council of Canada, Fonds de Recherche du Québec—Nature et Technologies, Alcoa and the Aluminium Research Centre—REGAL. The assistance of Edmond Rousseau at Laval University is gratefully acknowledged. The authors would also like to extend their appreciation to Guillaume Gauvin and Hugues Ferland for their technical support.

REFERENCES

1. Srinivasan, S.; Bommaraju, T. Electrochemical Technologies and Applications. In Fuel Cells: From Fundamentals to Applications; Springer: New York, NY, USA, 2006; pp. 98–186.

2. Fischer, W.K.; Perruchoud, R.C. Factors influencing the carboxy- and air-reactivity behavior of prebaked anodes in hall-heroult cells. In Proceedings of the Light Metals 1986—TMS 1986: 115th Annual Meeting, New Orleans, LA, USA, 2–6 March 1986; Minerals, Metals and Materials Society: New Orleans, LA, USA, 1986; pp. 575–580.
3. Keller, F.; Mannweiler, U.; Knall, E. Anode for the aluminum industry. In Constructing and Operating Anode Plants: What Top Management Needs to Know; R & D Carbon Ltd.: Sierre, Switzerland, 1995; pp. 217–224.
4. Eidet, T. Reactions on Carbon Anodes in Aluminium Electrolysis. Ph.D. Thesis, Norwegian University of Science and Technology, Trondheim, Norway, October 1997.
5. Vitchus, B.; Cannova, F. Pratical air reactivity impacts on anode performance. In Proceedings of the Light Metals 2002—TMS 2002: 131st TMS Annual Meeting, Seattle, WA, USA, 17–21 February 2002; Minerals, Metals and Materials Society: Seattle, WA, USA, 2002; pp. 553–559.
6. Lustenberger, M. Heat treatment of anodes for the Aluminium Industry. In Institut des Matériaux; Faculté Sciences et Techniques de l'Ingénieur: Lausanne, Switzerland, 2004; p. 143.
7. Bensah, Y.D.; Foosnaes, T. The Nature and Effect of Sulphur Compounds on CO2 and Air Reactivity of Petrol Coke. ARPN J. Eng. Appl. Sci. 2010, 5, 35–43.
8. Sørlie, M.; Eidet, T. The influence of pitch impurity content on reactivity of binder coke. In Proceedings of the Light Metals 1998—TMS 1998: 127th Annual Meeting and Exhibition, San Antonio, TX, USA, 15–19 February 1998; Minerals, Metals and Materials Society: San Antonio, TX, USA, 1998; pp. 763–768.
9. Farr-Wharton, R.; Welch, B.J. Chemical and electrochemical oxidation of heterogeneous carbon anodes. Electrochim. Acta 1980, 25, 217–221.
10. Tordai, T. Anode dusting during the electrolytic production of aluminum. In Falculté des Sicences et Techniques des Matériaux; Ecole Polytechnique Fédérale de Lausanne: Lausanne, Switzerland, 2007; p. 331.
11. Rolofs, B.; Poi, N.W. The effect of anode spike formation on operational performance. In Proceedings of the Light Metals 2000—TMS 2000: 129th TMS Annual Meeting TMS Annual Meeting, Nashville, TN, USA, 12–16 March 2000; Minerals, Metals and Materials Society: Nashville, TN, USA, 2000; pp. 535–540.
12. Gudmundsson, H. Anode dusting from a potroom perpective at nordural and correlation with anode properties. In Proceedings of the Light Metals 2011—TMS 2011: 141th Annual Meeting and Exhibition, San Diego, CA, USA, 27 February–3 March 2011; Minerals, Metals and Materials Society: San Diego, CA, USA, 2011; pp. 471–476.
13. Jahedi, M.; Oh, A.; Gulizia, E.; Gulizia, S.; Mallah, A.J. Anode coating to prevent airburn in aluminium smelters. In Proceedings of the Light Metals 2009—TMS 2009: 138th Annual Meeting and Exhibition, San Francisco, CA, USA, 15–19 February 2009; Minerals, Metals and Materials Society: San Francisco, CA, USA, 2009; pp. 951–955.
14. Lee, Y.J.; Radovic, L.R. Oxidation inhibition effects of phosphorus and boron in different carbon fibrics. Carbon 2003, 41, 1987–1997.
15. Durkic, T.; Peric, A.; Lausevic, M.; Dekanski, A.; Neskovic, O.; Veljkovic, M.; Lausevic, Z. Boron and phosphorus doped glassy carbon: I. Surface propertie. Carbon 1997, 35, 1567–1572.
16. Kowbel, W.; Huang, Y.; Tsou, H. Effect of boron ion implantation on the oxidation behaviour of three-dimensional carbon-carbon composite. Carbon 1993, 31, 355–363.
17. Radovic, L.R.; Karra, M.; Skokova, K.; Thrower, P.A. The role of substitutional boron in carbon oxidation. Carbon 1998, 36, 1841–1854.
18. Howe, J.Y.; Jones, L.E. Influence of boron on structure and oxidation behaviour of graphite fiber, P120. Carbon 2004, 42, 461–467.
19. Zhong, D.H.; Sano, H.; Uchiyama, Y.; Kobayashi, K. Effect of low-level boron doping on oxidation behaviour of polymide-derived carbon films. Carbon 2000, 38, 1199–1206.

20. Hagio, T.; Nakamizo, M.; Kobayashi, K. Studies on X-ray diffracton and Raman sectra of B-doped natural graphite. Carbon 1989, 27, 259–263.
21. Xianxian, W.; Radovic, L.R. Inhibition of catalytic oxidation of carbon/carbon composites by boron-doping. Carbon 2005, 43, 1768–1777.
22. Jonse, L.E.; Thrower, P.A. Influence of boron on carbon fiber microstructure, physical properties and oxidation behaviour. Carbon 1991, 29, 251–269.
23. Jonse, L.E.; Thrower, P.A. The effect of boron on carbon-fiber microstructure and reactivity. J. Chim. Phys. Phys. Chim. Biol. 1987, 84, 1431–1438.
24. Sogabe, T.; Nakajima, K.; Inagaki, M. Effect of boron-doping on structure and some properties of carbon-carbon composite. J. Mater. Sci. 1996, 31, 6469–6476.
25. Manganiello, F.; Duruz, J.-J.; Bello, V. Treating Prebaked Carbon Components for Aluminum Production, The Treated Components Thereof, and the Components Use in an Electrolytic Cell. U.S. Patent 5,486,278, 28 March 1994.
26. Sekhar, J.A.; Liu, J.J.; Duruz, J.-J. Carbon Bodies Resistant to Deterioration by Oxidizing Gases.U.S. Patent 5,753,382, 10 January 1996.
27. Sekhar, J.A.; Liu, J.J.; Duruz, J.-J. Carbon Bodies Resistant to Deterioration by Oxidizing Gases.U.S. Patent 5,985,114, 15 September 1997.
28. Bello, V.A.; Duruz, J.-J.; Manganiello, F.A. Treating Prebaked Carbon Anodes for Aluminium Production. European Patent 0,701,635, 1 June 1994.
29. Tosta, M.R.J.; Inzunza, E.M.; Delgado, L.A. Boron salt inhibitors of air reactivity of prebaked carbon anodes—Literature review and laboratory study. In Proceedings of the Light Metals 2009—TMS 2009: 138th Annual Meeting and Exhibition, San Francisco, CA, USA, 15–19 February 2009; Minerals, Metals and Materials Society: San Francisco, CA, USA, 2009; pp. 1173–1176.
30. Mirtchi, A.A.; Bergeron, J. Method for Providing a Protective Coating for Carbonaceous Components of An Electrolysis Cell. U.S. Patent 6,475,358, 6 February 2001.
31. Babaei, F.; Hong, T.L.C.; Yeung, K.; Cheng, S.H.; Lam, Y.W. Contrast-enhanced X-ray micro-computed tomography as a versatile method for anatomical studies of adult zebrafish. Zebrafish 2016, 13, 310–316.
32. Cnudde, V.; Boone, M.N. High-resolution X-ray computed tomography in geosciences: A review of the current technology and applications. Earth Sci. Rev. 2013, 123, 1–17.
33. Helliwell, J.R.; Sturrock, C.J.; Grayling, K.M.; Tracy, S.R.; Flavel, R.J.; Young, I.M.; Whalley, W.R.; Mooney, S.J. Applications of X-ray computed tomography for examining biophysical interactions and structural development in soil systems: A review. Eur. J. Soil Sci. 2013, 64, 279–297.
34. Mazonakis, M.; Damilakis, J. Computed tomography: What and how does it measure? Eur. J. Radiol. 2016, 85, 1499–1504.
35. Adams, A.N.; Karacan, O.; Grader, A.; Mathews, J.P.; Halleck, P.M.; Schobert, H.H. The non-destructive 3-D characterization of pre-baked carbon anodes using X-ray computerized tomography. In Proceedings of the Light Metals 2002—TMS 2002: 131st TMS Annual Meeting, Seattle, WA, USA, 17–21 February 2002; Minerals, Metals and Materials Society: Seattle, WA, USA, 2002; pp. 535–539.
36. Sommerseth, C.; Thorne, R.J.; Rørvik, S.; Sandnes, E.; Ratvik, A.P.; Lossius, L.P.; Linga, H.; Svensson, A.M. Spatial methods for characterising carbon anodes for aluminium production. In Proceedings of the Light Metals 2015—TMS 2015: 144th Annual Meeting and Exhibition, Orlando, FL, USA, 15–19 March 2015; Minerals, Metals and Materials Society: Orlando, FL, USA, 2015; pp. 1141–1146.
37. Picard, D.; Alamdari, H.; Ziegler, D.; Dumas, B.; Fafard, M. Characterization of prebaked carbon anode samples using X-ray computed tomography and porosity estimation. In Proceedings of the Light Metals 2012—TMS 2012: 141st Annual Meeting and Exhibition, Orlando, FL, USA, 11–15 March 2012; Minerals, Metals and Materials Society: Orlando, FL, USA, 2012; pp. 1283–1288.

38. Azari, K.; Alamdari, H.; Aryanpour, G.; Picard, D.; Fafard, M.; Adams, A. Mixing variables for prebaked anodes used in aluminum production. Powder Technol. 2013, 235, 341–348. [CrossRef]
39. Suriyapraphadilok, U.; Halleck, P.; Grader, A.; Andresen, J.M. Physical, chemical and X-ray computed tomography characterization of anode butt cores. In Proceedings of the Light Metals 2005—TMS 2005: 134th TMS Annual Meeting, San Francisco, CA, USA, 13–17 February 2005; Minerals, Metals and Materials Society: San Francisco, CA, USA, 2005; pp. 617–621.